UCU
university college utrecht

Universiteit Utrecht

Bachelor Thesis

Scanning Tunneling Microscopy and the production of atomically sharp tips

Frank Westhoek
3978257

24 June 2015

Supervisor

Dr. I. Swart
Condensed Matter and Interfaces,
Debye Institute for Nanomaterials Science

Coordinator

Dr. G.J. Vroege
University College Utrecht

Electrochemical etching and field-directed sputter sharpening production of atomically sharp tungsten tips for scanning tunneling microscopy

Frank Westhoek*, Marlou Slot, Nadine van der Heijden and Ingmar Swart
*Utrecht University, Debye Institute for Nanomaterials Science. *Corresponding author: f.westhoek@students.uu.nl*
(received 24 June 2015)

One of the great challenges of scanning tunneling microscopy is the production of atomically sharp tips. In this research, we have produced STM tips by electrochemical etching and subsequent field-directed sputter sharpening. Tips produced using these techniques were characterized using transmission electron microscopy. Here, we show that we have successfully produced atomically sharp tungsten tips with an apex radius of up to 1.4 nm. Although we have been able to reproduce field-directed sputter sharpening of tungsten tips, it remains unclear under which circumstances this method yields the best results. We suggest further systematical research in order to optimize this promising STM tip production technique.

Keywords: electrochemical etching; field-directed sputter sharpening; scanning tunneling microscopy; atomically sharp tips

I. INTRODUCTION

There exists a direct relationship between the quality and geometric characteristics of tips used in scanning tunneling microscopy (STM) and the quality of the images obtained [1]. In order to obtain high quality images, the production of excellent tips is thus quintessential. Many different production methods for STM tips exist [2]. Although most research groups use electrochemical etching, various other procedures are also used to produce tips. A single best production procedure yielding reliable and cheap tips of the highest quality does not yet exist, although efforts are undertaken to systematically study the optimal parameters for batch production of electrochemically etched STM tips [3]. The success rate seems to depend largely on the skills of the operator, and the production of atomically sharp tips has therefore been called to be more of an "art than a science" [4]. Quite recently, a new method called field-directed sputter sharpening has been published which offers several advantages over electrochemical etching: the process is self-limiting, suitable for batch production, efficient and cheap and produces tips of higher quality than previous methods [5,6]. In this research, we have sought to devise a reliable procedure for atomically sharp STM tip production and to reproduce the field-directed sputter sharpening technique.

A. Electrochemical etching

The electrochemical etching (ECE) of STM tips is a process in which a metal wire is partially dissolved in an electrolyte solution such that a sharp tip is formed. ECE is currently the most practical method for producing STM tips since it is able to produce cheap, reliable STM-tips of reasonable quality while the process is relatively easy and fast. Typical tip radii produced by ECE range between 4-50 nm [3,7,8]. For tungsten wires, both NaOH or KOH can be used for the electrolyte solution and there does not seem to be a clear preference in the literature for either substance or specific concentration [2,4,7,9]. Typically, the tungsten wire will have a diameter of around 0.3 mm, the applied voltage is around 3V and the etching process takes around 10 minutes, although times as short as a minute and up to 50 minutes are reported [2,4,10]. The following chemical reaction takes place during electrochemical etching:

$$\begin{array}{ll} \textit{cathode:} & 6H_2O + 6e^- \rightarrow 3H_2\,(g) + 6OH^- \\ \textit{anode:} & W\,(s) + 8OH^- \rightarrow WO_4^{2-} + 4H_2O + 6e^- \\ \hline & W\,(s) + 2OH^- + 2H_2O \rightarrow WO_4^{2-} + 3H_2\,(g) \end{array}$$

A tip is formed during the etching process because the electrolytic solution's surface tension will form a meniscus around the tungsten wire emerged in it. The concentration of OH^- ions is lower near the top of the meniscus than in the solution overall. The etching process thus takes place at a slower rate at the top of the meniscus. Where etching takes place at a higher rate, tungsten anions are formed that will flow downwards. This hinders the electrochemical etching of the tungsten wire submerged below the meniscus. Thus, a so-called 'neck-in' will occur close to the bottom of the meniscus. Eventually, the submerged part of the tungsten wire will become too heavy and the 'drop-off' occurs. At the breaking point, the sharp tip is formed. The formation and shape of the meniscus is thus crucial for electrochemical etching. It was experimentally confirmed that altering the meniscus shape, e.g. by lifting the wire during the process, will also alter the shape of the tip [3]. Because of the crucial shape of the meniscus, the ECE set-up should be kept free of external vibrations. The neck-in and drop-off process are depicted in Figures 1 and 2.

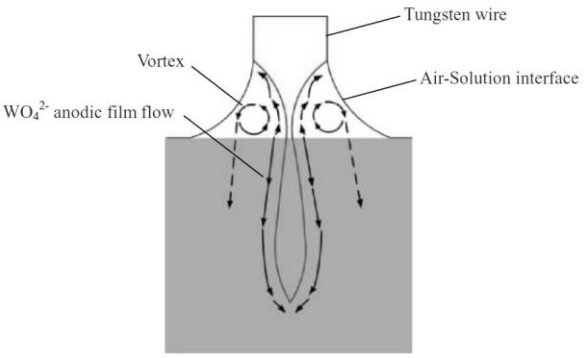

Figure 1. Schematic view of the neck-in process due to the tungsten anion flow around the meniscus [3].

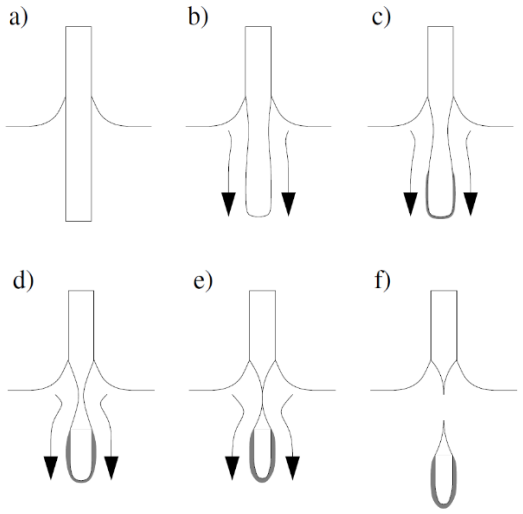

Figure 2. The drop-off process as a result of the neck-in process and the weight of submerged wire. The meniscus is formed in a); b) to e) show the tungsten anion flow; f) the drop-off [4].

ECE is not self-limiting and continuing to apply a voltage after the drop-off has occurred blunts the tip. Many papers therefore describe a mechanism that automatically cuts of the applied voltage within 500 ns after the drop-off has occurred [9]. Alternatively, the lower part of the tungsten wire also forms a tip at the drop-off, and the blunting process does not affect this submerged STM-tip [7]. By designing the production device in such a way that these submerged tips are recollected undamaged, sharp tips can also be produced [11–13].

Most papers describing ECE procedures use a tungsten wire, which unfortunately suffers from oxidation (mostly WO_3) [14]. The storage of these tips after production is therefore problematic since oxidation will take place if stored under ambient conditions [7]. This does not only affect the sharpness of the tip, but could destabilize the tunneling current as well [2]. Typically, the oxidation layer is around 2 nm in thickness [7,9].

B. Field-directed sputter sharpening

Field-directed sputter sharpening (FDSS) can be applied to electrochemically etched STM tips in order to further sharpen them. The technique is similar in principle to conventional sputter erosion (CSE), in which a metallic tip is sharpened due to ion bombarding under an angle. However, CSE is not able to produce the ultrasharp tips desired for use in STM [5,15]. Field-directed sputter sharpening bombards Argon ions onto a metallic STM tip, but during the process a bias is applied to the tip. This produces a spatially localized repulsive potential at the apex of the tip (see Figure 3). The electric field gets localized more strongly as the apex narrows, thus ions directed at the sharpest part of the tip will undergo the most deflection [5]. This subsequently leads to an even further reduction of the ion flux at the apex which produces a sharp apex due to directed sputter sharpening.

In comparison to CSE, FDSS produces significantly sharper tips [5,16]. In CSE, there is a competition between erosional sharpening and blunting of the tip. By field-direction, FDSS produces an equilibrium curvature of the tip that depends on the ion flux. The deflection of ions also preserves the structural integrity of the tip base which is of importance to tip stability. Ultimately, a tip apex equilibrium is reached in FDSS where ion sputtering continues without influencing the apex.

II. EXPERIMENTS, RESULTS AND DISCUSSION

A. Tip production (ECE) and characterization

Tungsten tips are produced from a polycrystalline tungsten wire (ChemPur; 0.25 mm diameter, 99.95+%). Tips are produced using a simple electrochemical etching set-up modelled after the design of [7] which does not require a computer controlled power supply (see Figure 4). The wire is attached to a ring stand and threaded to a 2.4 mm hole in a stainless steel plate connected to a different ring stand. The length of the wire under the plate is a little over 1 cm. Underneath the stainless steel plate, a short plastic tube (<1 cm, small radius) is placed filled with paper flasks at the bottom. This will collect the lower part of the wire after the drop-off has occurred and its length and diameter should be such that the collected tip will not touch the sides of the tube once collected. The tungsten wire (anode) and stainless steel plate (cathode) are now connected to the DC power supply. A small droplet of 2M NaOH etching solution is placed in the hole, and a 3V DC voltage is now applied. After the drop-off has occurred, the power supply is switched off manually. The tip is collected and rinsed in distilled water and ethanol subsequently.

Electrochemically etched tips were then studied using an

optical microscope attached to a computer to study their macroscopic geometry. Since field-directed sputter sharpening requires straight tips, clearly deformed (e.g. bent) tips should be recognized a priori to improve FDSS yield. Using a transmission electron microscope (TEM) (Philips Tecnai 10; 100 kV), more detailed images of the tips were collected. The chemical composition of the electrochemically etched tips and possible contaminations/oxidation layers were studied using Energy Dispersive X-Ray (EDX) analysis integrated in a TEM system (Phillips Tecnai 20F; 200 kV). We have used a spherical approximation for final tip apexes and hence quantified tip sharpness using the radius of curvature of the final tip apex. If a well-defined oxidation layer was present, we defined the tip radius at the sub-surface tungsten core apex.

B. Tip sharpening (FDSS)

After TEM characterization, electrochemically etched tungsten tips were brought into a high-vacuum antechamber (below $2 \cdot 10^{-9}$ mbar) of the STM (Scienta Omicron Fermi SPM). Tips were placed in STM tip holders that were put in a tip carrier. A custom-made holder for this carrier was placed in the antechamber and connected to an external power supply (Delta Electronics SM 400-AR-8). A bias of 400 V (relative to ground) was applied to this holder which was electrically isolated from the rest of the chamber. An Omicron ISE 10 Sputter Ion Source (variable acceleration voltage, 2 cm beam diameter) was used for the sputter sharpening and placed some 5 cm from the tip. Sputtering was applied for approximately 60 minutes using the standard focus/extractor profile of the sputter gun. During sputtering, the Argon pressure was kept around $3.0 \pm 0{,}1 \cdot 10^{-6}$ mbar. After field-directed sputter sharpening, tips could either be directly used in STM experiments or removed from the vacuum system for TEM characterization.

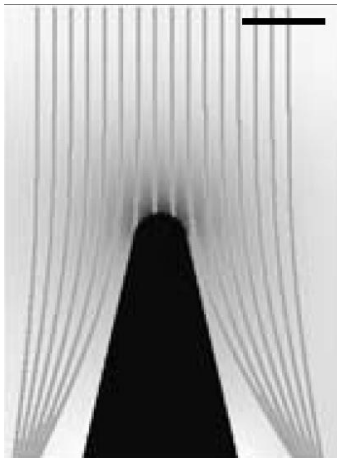

Figure 3. Simulation of field-directed sputter etching around a biased tip apex (greyscale represents strength of electric field, lines the paths of individual ions, scale bar: 20 nm) [5]

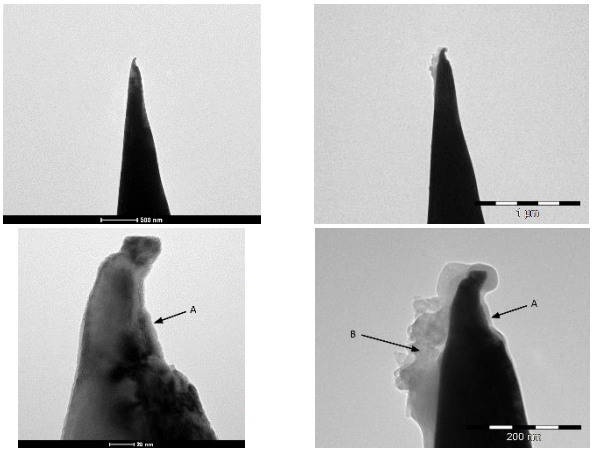

Figure 5. Typical tip produced with ECE (7 nm radius) shown at two different scales. TEM images (left) were taken approximately one hour after etching, whereas TEM images (right) were taken four days later. Growth of the (presumptive) oxidation layer (A) is clearly visible ,whereas even more contamination is observed on the left-hand side (B).

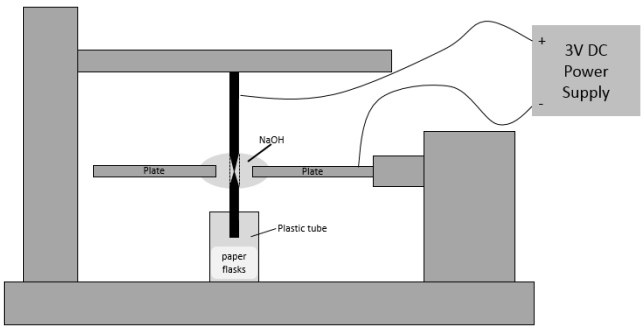

Figure 4. Sketch of electrochemical etching set-up (not to scale).

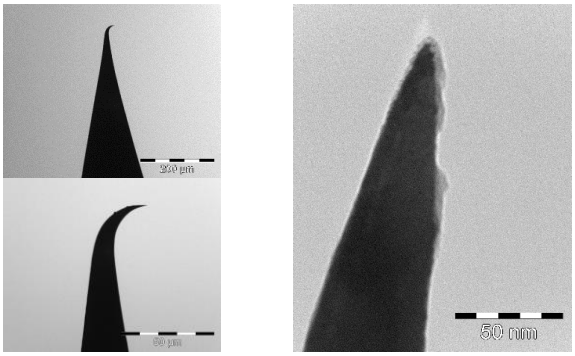

Figure 6. The sharpest tip produced in this research (1.4 nm radius) with an oxidation layer of around 1-2 nm thickness surrounding the tip. Due to the macroscopic shape of this tip (bent tip apex), it is not fit for FDSS.

Table I. Tip radius before and after field-directed sputter sharpening.
E_{ion} = ion energy; V_{probe} = probe bias; $E_{relative}$ = ion energy – probe bias; $V_{relative}$ = probe bias/ion energy

Tip	Radius before FDSS (nm)	Radius after FDSS (nm)	Difference	E_{ion} (V)	V_{probe} (V)	$E_{relative}$ (V)	$V_{relative}$
A	10	4	-6	1500	150	1350	0.1
B	5	104	+99	1500	150	1350	0.1
C	25	36	+11	1778	178	1600	0.1
D	12	N/A	N/A	1222	122	1100	0.1
E	38	10	-28	1500	150	1350	0.1
F	18	13	-5	1500	150	1350	0.1

Table II. Average radius and cone angle of STM tips after ECE.

	Radius (nm)	Cone angle (°)
Average	15.5	33.7
Minimum	1.4	12
Maximum	62	95
Standard Deviation	15.3	20.4

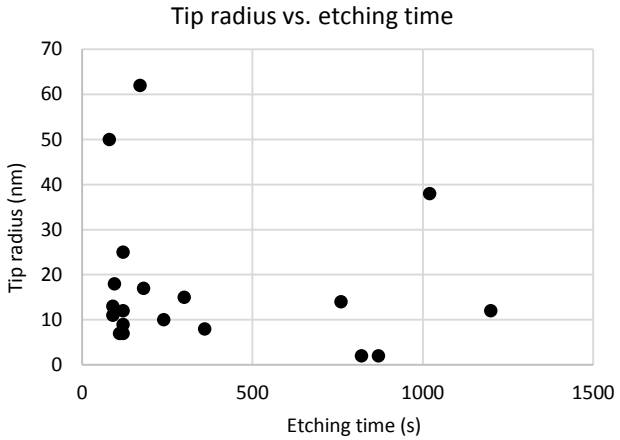

Figure 7. Tip radius (nm) vs. etching time (s) of electrochemically etched tungsten tips. There does not seem to be a relationship between tip etching time and tip radius.

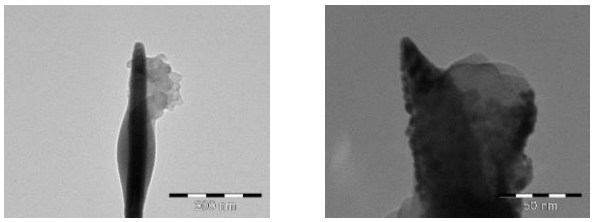

Figure 8. Tip A before (left) and after (right) FDSS. The tip radius was reduced from 10 nm to 4 nm.

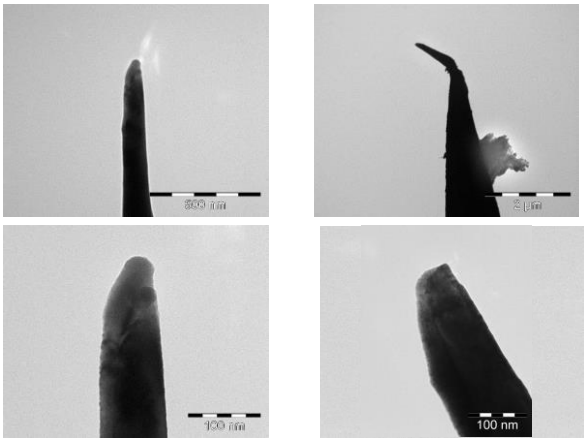

Figure 9. Tip C before (left, two scales) and after (right, two scales) FDSS. Due to the bent tip apex, FDSS field lines were probably distorted and tip radius was increased from 25 nm to 36 nm.

C. Results and discussion

We have produced and characterized 23 electrochemically etched tips. The important characteristics of these tips are listed in Table II and a typical tip is shown in Figure 5. Our results are in close agreement with earlier studies, although our best tip is considerably sharper than previous studies (1.4 nm vs 4 nm, see Figure 6) [3,7]. This exceptional result could not be surpassed by tips treated with FDSS, but we were not able to routinely reproduce this result with ECE either. The average tip radius achieved in this research is good although the deviation around this average is still relatively large and the procedure would thus need to be improved before it is suitable for batch production. As can be inferred from Figure 7, ECE typically lasted for 1-4 minutes or 11-16 minutes. There does not seem to be a clear relationship between tip etching time and tip radius.

The chemical reaction involved in ECE behaved differently from time to time. The gaseous bubble formation of the hydrogen gas could take place more violently (shorter reaction times) or calmly (longer reaction times). More research into the underlying mechanisms dictating the reaction rate of tungsten ECE is necessary to understand this phenomenon better.

Tips produced using electrochemical etching were stored under ambient conditions and hence suffered from oxidation. Furthermore, despite rinsing in distilled water and ethanol, other contaminations (e.g. from the etching solution) could still be present. Oxidation and other contaminations were present in virtually every tip studied in this research. An oxidation layer is clearly visible in Figure 5 and 6 and Figure 8 shows other contaminations. EDX analysis was performed in order to determine the chemical

composition of these contaminations. The presumptive oxidation layer visible in Figures 5 and 6 could not reliable be resolved using EDX. The layer is very thin and thus hard to resolve due to resolution limitations. Furthermore, the tip can be idealized as a spherical cone. An oxidation layer would also be present in the middle of the tungsten tip (top view) since this merely represents the uppermost part of the spherical cone in real space. Therefore the difference in chemical composition between a spot at the center of the tungsten tip and along the edges at the oxidation layer are expected to be minimal, even if resolution limitations would not play a role. Later tips that were stored in a vacuum exsiccator (under nitrogen atmosphere) after ECE showed considerably less oxidation.

The chemical composition of larger contaminations such as those in Figure 8 could be resolved using EDX. The data shows presence of carbon, oxygen, copper, iron, aluminium, sodium, chloride, sulfur, calcium and tungsten. The presence of carbon, oxygen and sodium is easily explained, since contamination of hydrocarbons, etching residuals and tungsten oxides is in accordance with the literature [2,7,17]. Since the TEM sample holder is made out of copper, the presence of copper in the spectrum was expected. Why the tip was contaminated with iron, aluminium, chloride, sulfur and calcium remains unclear.

Field-directed sputter sharpening was applied to 8 tips in total, out of which 6 were TEM characterized (1 was lost; 1 was used immediately in STM imaging). As can be inferred from Table I, FDSS resulted in tip sharpening in 3 out of 6 cases. Judging from TEM images, it is likely that tips B and D were severely damaged before or after FDSS and as a result of this no sharpening is visible on the TEM images. Tips were manually processed and transported to the electron microscope, thus damage resulting from this is not unlikely. FDSS yield is hence expected to be substantially higher if tips are immediately used for STM imaging. Tip C was slightly bent at the top, and it is therefore likely that FDSS had a different effect on this tip than anticipated due to distorted field lines. We conclude that we have been able to successfully reproduce field-directed sputter sharpening of tungsten STM tips. Comparisons between the tip before FDSS (left) and after FDSS (right) are shown for tip A (Figure 8) and C (Figure 9).

Although our results show that we have been able to reproduce FDSS, the effect was smaller than anticipated upon the basis of earlier research [5,16]. We believe several factors have influenced this. Firstly, the sputter pressure in this research ($3.0 \pm 0{,}1 \cdot 10^{-6}$ mbar) was considerably lower than in previous research ($7.3 \cdot 10^{-5}$ mbar). Since our equipment is too sensitive to be used at such pressures, we had to use lower sputter pressures. However, since sputter pressure together with ion energy dictate the 'sputter rate',

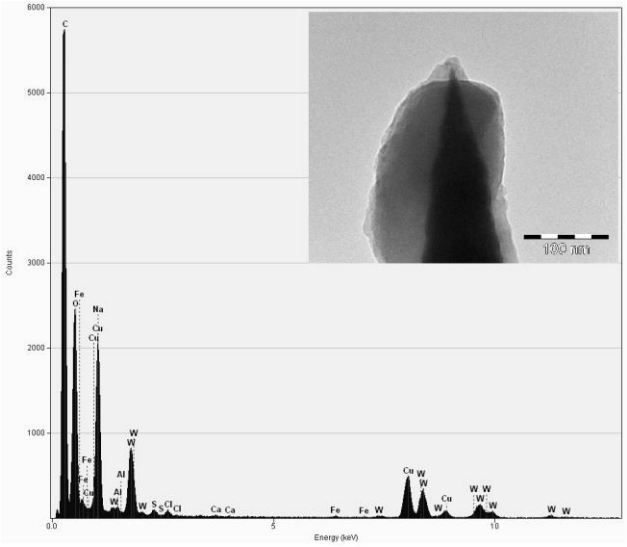

Figure 10. EDX spectrum of a heavily contaminated tip (inset, tungsten tip apex radius of 2 nm).

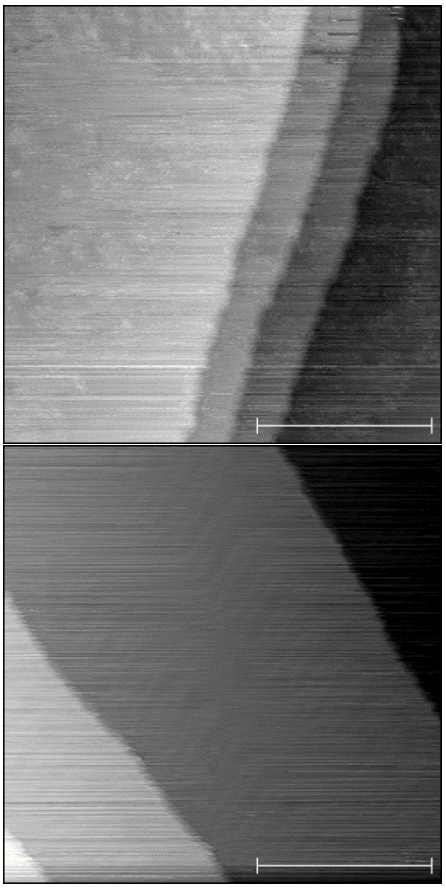

Figure 11. STM images (100x100 nm) of the surface of a Au (111) crystal before (top image) and after (bottom image) FDSS. Herring bones are clearly visible in the image obtained with a sputtered tip. Images were collected with the Omicron Fermi STM using the following parameters: V-gap = 0.1 V; I-setpoint = 1 nA; Loop gain = 3% (trace down). Images were processed using Gwyddion; inter alia, linewise plane subtraction was applied. Scale bar = 40 nm.

this could partially explain the observed difference in sharpening. Considerable longer sputter times may compensate for the lower sputter pressure, but this still needs to be experimentally confirmed. Secondly, we believe that the electric field lines of our tips were not nearly as well-defined as modelled in Figure 3 [5]. Tips were placed in tip holders of the Omicron SPM Fermi model STM that were placed in tip carriers during sputtering. The tip did not protrude above the electrically conductive tip carrier. The tip carrier is likely to have influenced the electric field lines which are crucial for FDSS to form a sharp tip. The distortion due to the tip carrier is twofold; the Argon ions will be deflected differently resulting in a different FDSS effect and the field lines resulting from the tip carrier are likely to have decreased the kinetic energy of the Argon ions as well. We hypothesize that the combination of these two effects have influenced our results and explain the observed difference in sputter sharpening between our results and earlier results. This could be further researched with a different set-up, or by compensation for these effects within the current set-up upon the basis of computer modelling of the tip and tip carrier.

STM imaging was performed before and after FDSS using the same tip (see Figure 11). A clear improvement is visible, since in the image obtained with a FDSS-treated tip the herring bones of the Au(111) surface are visible a contrary to the image obtained with the tip before FDSS. Although too many factors influence STM imaging to conclude that this improvement is solely due to FDSS on the basis of one test, we can conclude with certainty that at least FDSS did not affect the STM imaging capability of the tip negatively, and quite possibly affected it positively.

III. CONCLUSIONS

We have successfully reproduced field-directed sputter sharpening of tungsten tips for use in scanning tunneling microscopy. The tip apex radius was substantially reduced in some of the cases where FDSS was applied. Our electrochemical etching set-up also yielded excellent results. This combination of techniques offers great potential for batch production of tips and subsequent detailed STM imaging given the relative simplicity of the methods employed, the cheap price of starting materials, and the high quality of final products. However, more research into the optimal FDSS parameters still needs to be carried out. Due to different (tip holder) designs of STM systems, it is likely that these parameters will differ per laboratory. Since reliable tips are the limiting factor in present-day STM imaging, this tip production technique offers researchers in nanotechnology great potential to improve STM imaging.

ACKNOWLEDGEMENTS

We thank J. van der Lit and C. Post for valuable discussions, S. Zevenhuizen for help with TEM imaging and H. Meeldijk for help with EDX/TEM imaging.

APPENDIX

Supplementary figures accompany this paper.

[1] ASTM International, Guide to Scanner and Tip Related Artifacts in Scanning Tunneling Microscopy and Atomic Force Microscopy, (2012) 1–18.

[2] Oliva, A.I., Romero G., A., Peña, J.L., Anguiano, E., Aguilar, M., Electrochemical preparation of tungsten tips for a scanning tunneling microscope, Rev. Sci. Instrum. 67 (1996) 1917-1920. doi:10.1063/1.1146996.

[3] Ju, B.F., Chen, Y.L., Ge, Y., The art of electrochemical etching for preparing tungsten probes with controllable tip profile and characteristic parameters, Rev. Sci. Instrum. 82 (2011). doi:10.1063/1.3529880

[4] Lucier, A. Preparation and Characterization of Tungsten Tips Suitable for Molecular Electronics Studies (MSc Thesis, McGill University: Montréal), (2004).

[5] Schmucker, S. W., Kumar, N., Abelson, J. R., Daly, S. R., Girolami, G. S., Bischof, M. R., ... & Lyding, J. W. (2012). Field-directed sputter sharpening for tailored probe materials and atomic-scale lithography, Nat. Commun. 3 (2012) 935. doi:10.1038/ncomms1907. [6] J. Lyding, News Microscope probe-sharpening technique improves resolution, (2012) 2012.

[7] Müller, A.-D., Müller, F., Hietschold, M. Demming, F., Jersch, J. Dickmann, K., Characterization of electrochemically etched tungsten tips for scanning tunneling microscopy, Rev. Sci. Instrum. 70 (1999) 3970–3972. doi:10.1063/1.1150022.

[8] Voigtländer, B., Scanning Probe Microscopy: Atomic Force Microscopy and Scanning Tunneling Microscopy. Berlin: Springer-Verlag (2015).

[9] O.L. Guise, J.W. Ahner, M.C. Jung, P.C. Goughnour, J.T. Yates, Reproducible Electrochemical Etching of Tungsten Probe Tips, Nano Lett. 2 (2002) 191–193. doi:10.1021/nl010094q.

[10] Kim P., Kim J.H., Jeong M.S., Ko D.K., Lee J., Jeong S., Efficient electrochemical etching method to fabricate sharp metallic tips for scanning probe microscopes, Rev. Sci. Instrum. 77 (2006). doi:10.1063/1.2358703.

[11] Klein M., Schwitzgebel G., An improved lamellae drop-off technique for sharp tip preparation in scanning tunneling microscopy, Rev. Sci. Instrum. 68 (1997) 3099. doi:10.1063/1.1148249.

[12] Bryant P.J., Kim H.S., Zheng Y.C., Yang R., Technique for shaping scanning tunneling microscope tips, Rev. Sci. Instrum. 58 (1987) 1115. doi:10.1063/1.1139618.

[13] Kulawik M., Nowicki M., Thielsch G., Cramer L., Rust H.P., Freund H.J., et al., A double lamellae dropoff etching procedure for tungsten tips attached to tuning fork atomic force microscopy/scanning tunneling microscopy sensors, Rev. Sci. Instrum. 74 (2003) 1027–1030. doi:10.1063/1.1532833.

[14] Lucier A.-S., Mortensen H., Sun Y., Grütter P., Determination of the atomic structure of scanning probe microscopy tungsten tips by field ion microscopy, Phys. Rev. B. 72 (2005) 1–9. doi:10.1103/PhysRevB.72.235420.

[15] Chaika, A.N., Orlova, N.N., Semenov, V.N., Postnova, E.Yu., Krasnikov, S.A., Lazarev, M.G., ... & Shvets, I.V., Fabrication of [001]-oriented tungsten tips for high resolution scanning tunneling microscopy., Sci. Rep. 4 (2014) 3742. doi:10.1038/srep03742.

[16] Lyding, J. W., & Schmucker, S. W. (2011). U.S. Patent No. 8,070,920. Washington, DC: U.S. Patent and Trademark Office

[17] Ekvall I., Wahlstrom, E., Claesson D., Olin H., Olsson E., Preparation and characterization of electrochemically etched W tips for STM, Doktorsavhandlingar Vid Chalmers Tek. Hogsk. 10 (2000) 11–18. doi:10.1088/0957-0233/10/1/006.

SUPPLEMENTARY FIGURES

1. Optical microscope images of tungsten tips
2. Photographs of electrochemical etching set-up
3. Tip characterization
4. Photographs of field-directed sputter sharpening set-up (STM)
5. TEM images of sputtered tips

Section 1 – Optical microscope images of tungsten tips

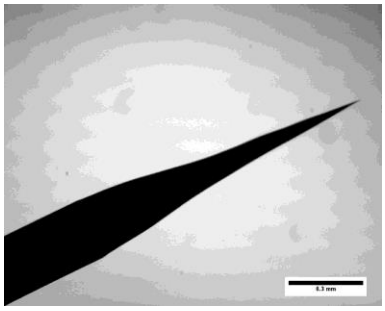

Figure 1.1. Optical microscope image of typical tip (bottom part) produced with electrochemical etching.

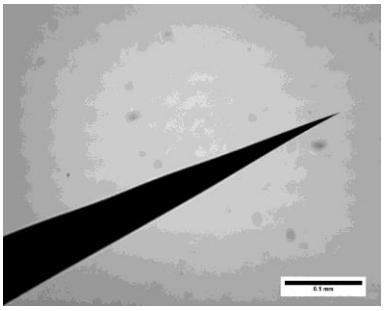

Figure 1.2. Optical microscope image of typical tip (bottom part) produced with electrochemical etching (zoom).

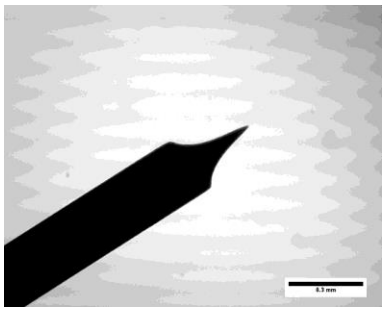

Figure 1.3. Optical microscope image of typical tip (upper part) produced with electrochemical etching.

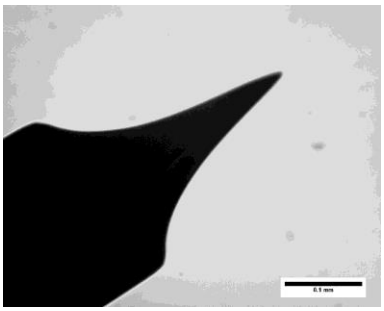

Figure 1.4. Optical microscope image of typical tip (upper part) produced with electrochemical etching (zoom).

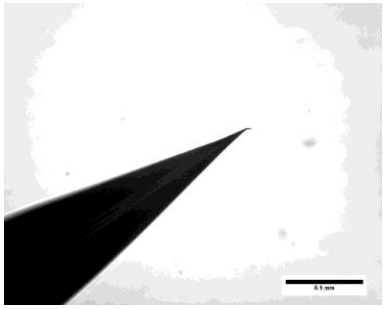

Figure 1.5. Optical microscope image of tip (upper part) less suitable for FDSS due to the macroscopic shape (bent apex).

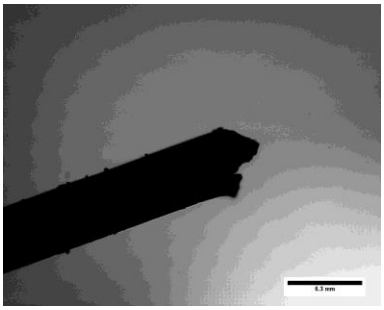

Figure 1.6. Optical microscope image of cut tungsten wire.

Section 2 – Photographs of electrochemical etching set-up

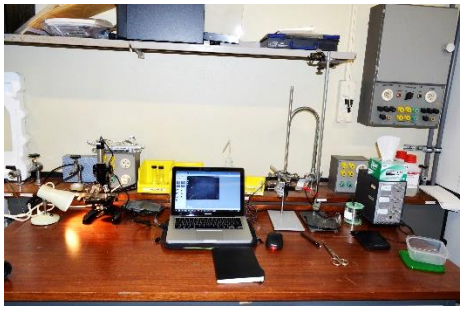

Figure 2.1. Electrochemical etching set-up (right) and optical microscope connected to computer (left).

Figure 2.2. The two ring stands, stainless steel plate and power supply of the ECE set-up.

Figure 2.3. Gaseous bubble formation during the etching.

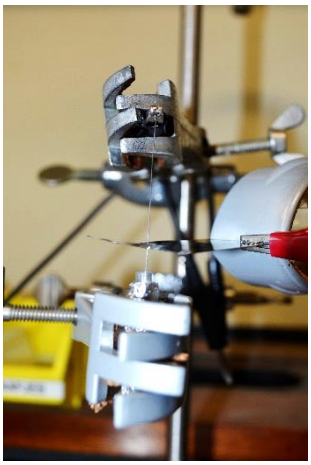

Figure 2.4. Detailed photograph of tungsten wire threaded through steel plate and flask for recollection of dropped-off tips.

Section 3 – Tip characterization

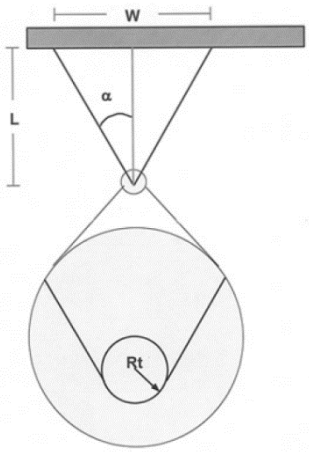

Figure 3.1. Definition of tip radius and cone angle.

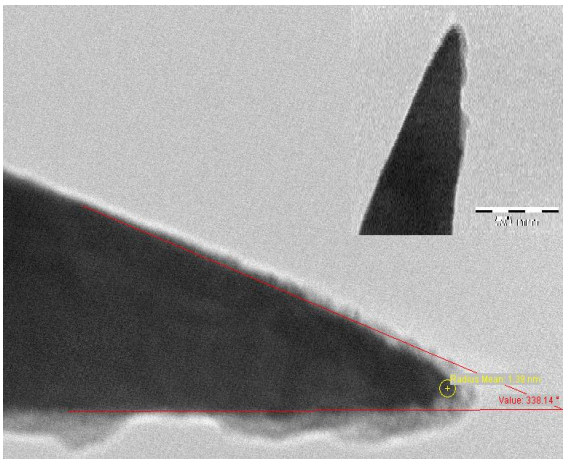

Figure 3.2. Tip radius was defined at the sub-oxidation layer level as depicted in this TEM image.

Section 4 – Photographs of field-directed sputter sharpening set-up (STM)

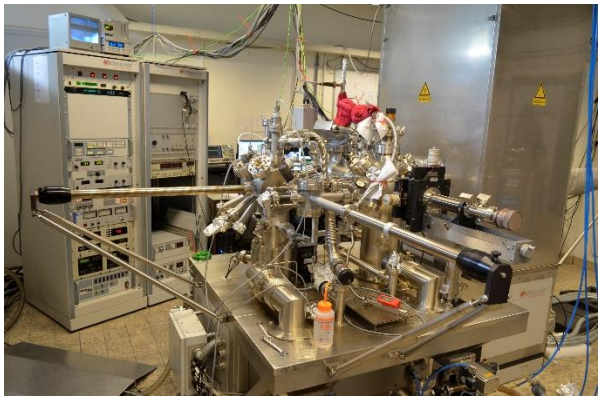

Figure 4.1. STM set-up in which the FDSS was performed.

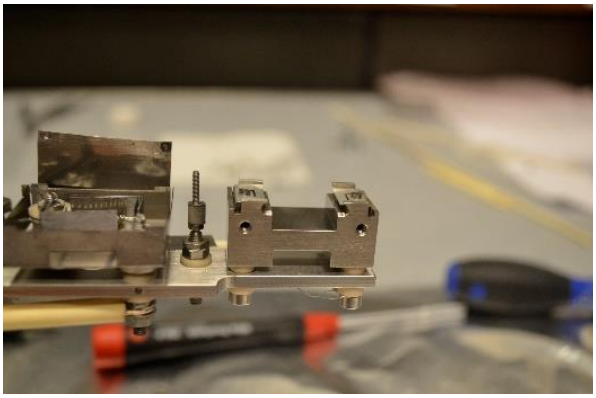

Figure 4.2. Custom-made holder for the tip carrier during assembly.

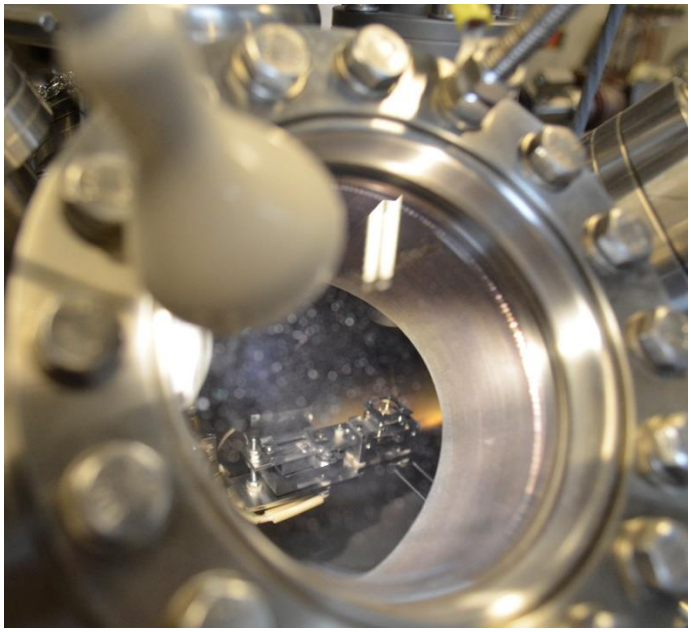

Figure 4.3. Tip carrier with tip in tip holder during sputtering in the ultra-high vacuum antechamber.

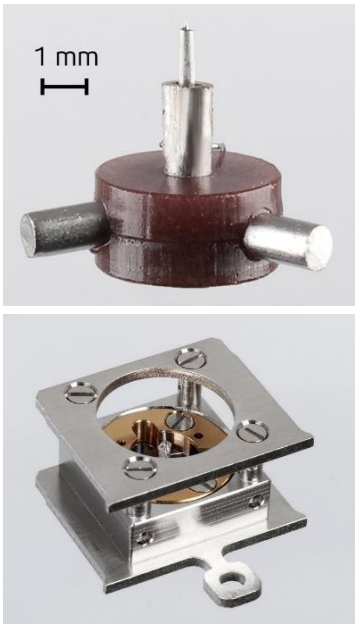

Figure 4.4. Tip holder and tip holder carrier. Source: scientaomicron.com

Section 5 – TEM images of sputtered tips

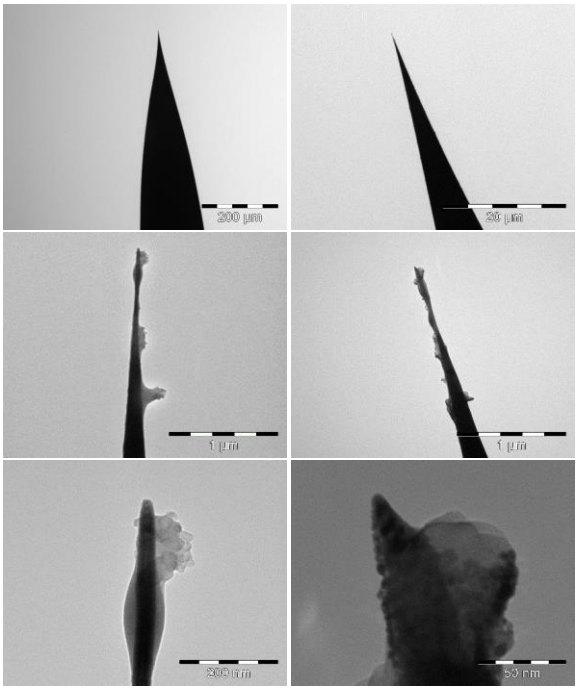

Figure 5.1. TEM images of tip A before (left) and after (right) sputtering. Tip radius was decreased from 10 to 4 nm.

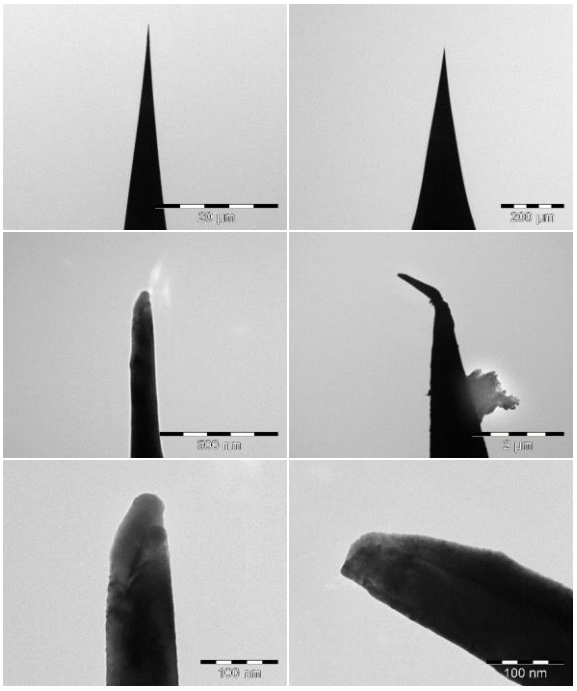

Figure 5.3. TEM images of tip C before (left) and after (right) sputtering. Tip radius was increased from 25 to 36 nm.

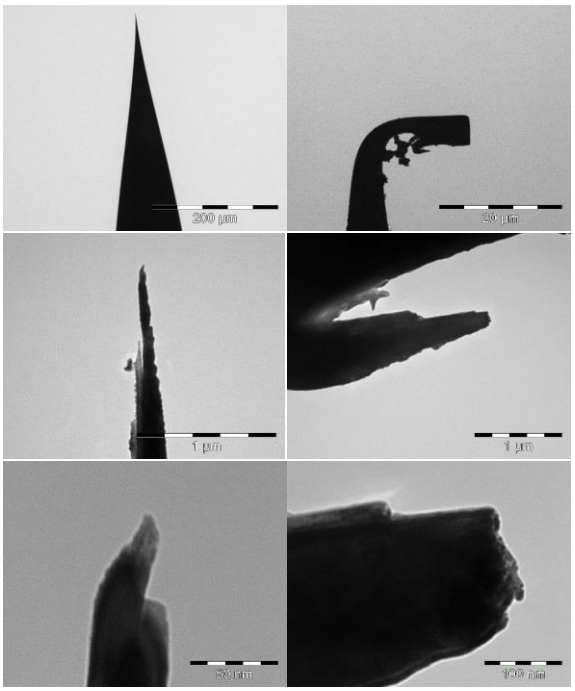

Figure 5.2. TEM images of tip B before (left) and after (right) sputtering. Tip radius was increased from 5 nm to 104 nm.

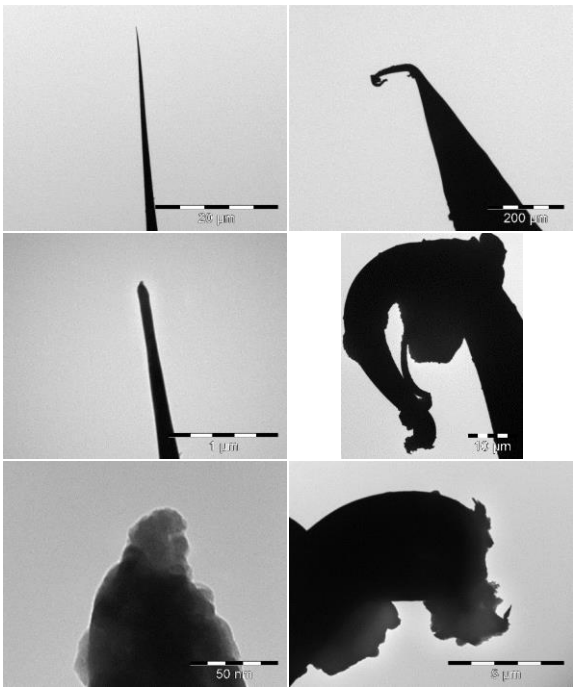

Figure 5.4. TEM images of tip D before (left) and after (right) sputtering. Tip radius was clearly increased, although no radius could be calculated..

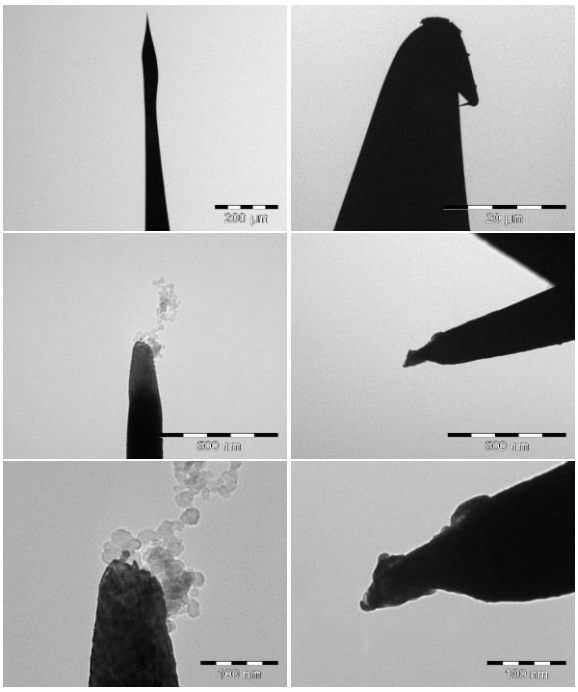

Figure 5.5. TEM images of tip E before (left) and after (right) sputtering. Tip radius was decreased from 38 to 10 nm.

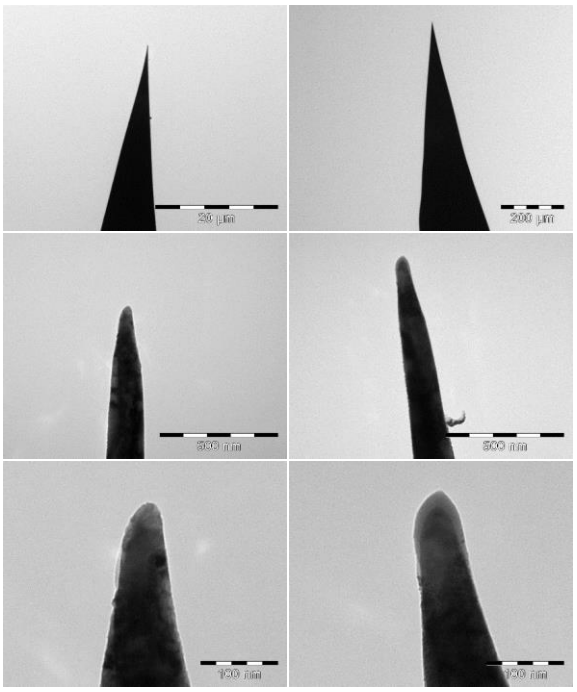

Figure 5.6. TEM images of tip F before (left) and after (right) sputtering. Tip radius was decreased from 18 to 13 nm.

LITERATURE REVIEW

Bachelor Thesis

Scanning Tunneling Microscopy and the production of atomically sharp tips

Frank Westhoek
3978257

Supervisor

11 May 2015

Dr. I. Swart
Condensed Matter and Interfaces,
Debye Institute for Nanomaterials Science

Coordinator

Dr. G.J. Vroege
University College Utrecht

INTRODUCTION

Scanning Tunneling Microscopy (STM) has quickly become one of the chief imaging techniques used for studies into nanoscale materials after its invention in the early 1980s by Gerd Binnig and Heinrich Roher. The technique allows for imaging and manipulation of single atoms and can be applied to a large variety of chemical compounds. Due to the invention of STM, a whole class of scanning probe microscopes now exist. Examples are atomic force microscopy, scanning thermal microscopy or ballistic-electron-emission microscopy [1]. STM does not depend on optical techniques but rather scans the relief of the compound using a sharp tip (needle). The production of these tips is one of the great challenges of this microscopy technique. There is a direct relationship between the quality and characteristics of the tip and the quality of the image obtained. In order to produce high quality images, the production of excellent tips is thus quintessential.

Different production methods for STM tips exist. Although most research groups use electrochemical etching, various other procedures are also used to produce such tips. A single best procedure yielding tips of the highest quality does not exist. The success rate still seems to depend largely on the skills of the operator, and the production of atomically sharp tips has thus been called to be more of an "art than a science" [2]. Recently, an alternative method called field-directed sputter sharpening has been published. This alternative method offers several advantages over conventional electrochemical etching and is thus of great interest to researchers.

This literature review will first discuss scanning tunneling microscopy in general and the quantum theory of STM. Tip characterization and production will then be discussed, followed by more detailed treatment of electrochemical etching production and field-directed sputter sharpening tip production. The literature review will be concluded with a brief description of the research that will be conducted for this bachelor thesis. The research will focus on reproducing the method of STM tip production by field-directed sputter sharpening, and more specifically to find the circumstances under which field-directed sputter sharpening yields tips of the highest quality.

SCANNING TUNNELING MICROSCOPY

The basic principle of scanning tunneling microscopy is comparable to reading braille. A sharp tip scans the surface of the compound in the x, y and z-direction using piezoelectric elements. It does so by placing the tip a few nanometers above the sample and applying a bias (voltage) to both the sample as the tip. A so-called tunneling current can now exist that strongly depends on the distance between the tip and the sample. Typically, a bias between 1 mV and 4V is applied to the tip which results in a tunneling current between 0.1 nA and 10 nA [3]. By sweeping over the compound (rastering) and monitoring this tunneling current, a surface image can be generated pixel by pixel. The tunneling current is due to quantum tunneling, which refers to the ability of particles to tunnel through a classically forbidden barrier. More detailed information on quantum tunneling can be found in the subsequent section.

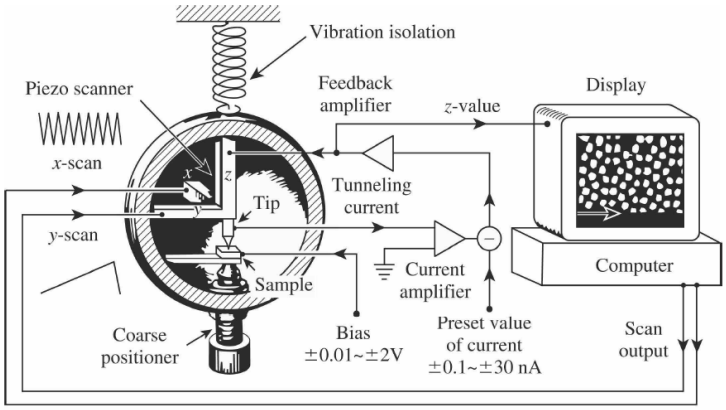

Figure 1. Fundamental components of an STM [4].

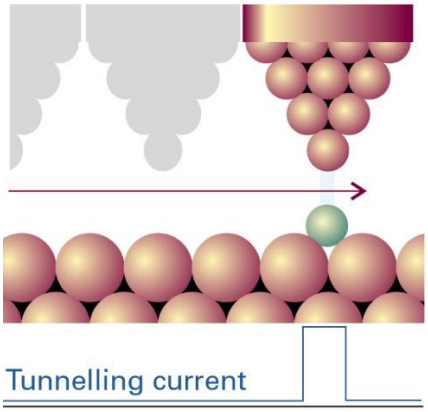

Figure 2. The scanning of a STM tip over the surface and the resulting tunneling current [5].

Figure 1 depicts the fundamental components of an STM and Figure 2 the working of the STM. The 3D piezoelectric scanner is both used to position the tip close to the sample before the experiment as to monitor the tunneling current/tip position during the experiment (depending on the mode of operation). It is composed out of three mutually perpendicular piezoelectric transducers or a piezoelectric tube that is able to move in three dimensions [4]. Such piezoelectric materials change dimensions in response to an applied voltage. Depending on the polarity of the voltage, they either contract or expand. The resulting small tunneling current from the tip is amplified and recorded. The feedback amplifier is subsequently used to adjust the tunneling current to match the preset value of the current in constant current mode. The coarse positioner is used to roughly position the sample and piezo scanner close to each other after which further positioning is done with the piezoelectric scanner. Lastly, the vibration isolation is of crucial importance due to the precision with which the STM has to function.

The great achievement of Binnig & Roher was that they were able to design a STM that was sufficiently protected against vibrations to perform precise microscopy [6]. The principle of STM had already been conceived, but before Binnig & Roher no one had succeeded in creating the device [7]. In their first successful attempt, they protected the tunneling unit by installing the vacuum chamber on a heavy stone bench, floating on inflated rubber tubes. Furthermore, the internal vibrations of the system were filtered out by static magnetic levitation of the tunneling unit [6]. The STM also had to be operated in a quiet environment. The vacuum used was around the order of 10^{-6} Torr, where other STMs operate around $2 \cdot 10^{-10}$ Torr [8]. An STM is always subject to external vibrations transmitted by air or the ground, and thus needs to be isolated from such vibrations. Machines, building and walking vibrations are all in the range between 1-100 Hz and the vibration reduction should focus on this frequency range primarily [1]. Typically, the vibrational noise signal is about 10.000 times larger than the signal to be measured [9]. The STM is placed within a vibration reduction system consisting of two stages suspended from springs in vacuum, with Eddy currents due to permanent magnets acting as the damping system. This system is usually placed upon a vibration isolation table to ensure optimal vibration isolation.

The strong dependence of tunneling current on distance was shown in Binnig & Roher's publication using Figure 3, which indeed shows that a 1 Å ($1 \cdot 10^{-10}$ m) vertical displacement results in a change in current of around an order of magnitude. The resolution of STM imaging can be approximated quite easily [10,11]. Even for a large radius of the tip (1000 Å) the resolution will be rather sharp though not atomic (50 Å). Resolutions considerably below 100 Å thus need tip radii of around 100 Å or lower [11]. Under favorable conditions, a resolution under 2 Å can be achieved [8].

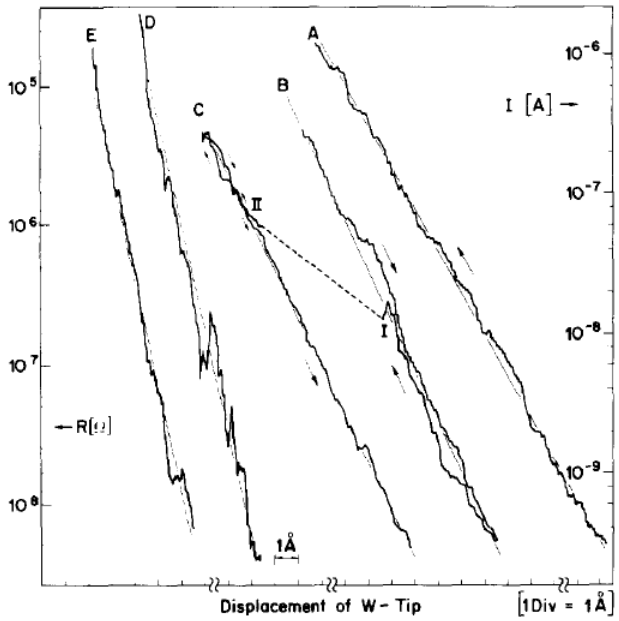

Figure 3. Tunneling resistance and current versus tungsten tip displacement, depicting the strong dependence of both the tunneling resistance and current on vertical displacement. For curves D and E (measured in vacuum), a 1 Å vertical displacement results in a change in current of around an order of magnitude [6].

Two main modes of STM operation exist; *constant current* mode or *constant height* mode [1]. In the constant current mode, the tip is vertically moved at each data point (x,y position) until a certain preset current value is reached. The voltage applied to the piezoelectric scanner needed for this constant tunneling current serves as a proxy variable for the vertical position of the tip [3]. If the sensitivity of the piezoelectric scanner is known, the topographic data can be acquired. The tip will then move to the next data point and move vertically until the predetermined current is reached. In the constant height mode, the distance between the tip and the sample is fixed and the tunneling current for every x,y data point is stored. The constant height mode offers much quicker imaging and is thus of interest when the data-collection time is limited, for example in dynamic processes. Quick imaging also reduces image distortion due to effects such as piezoelectric hysteresis and thermal drifts[1]. The constant height method is harder to employ though, since the tunneling function needs to be calibrated. The constant current mode is more commonly employed due to its main advantage that it is better able to scan surfaces that are not atomically flat.

[1] The sensitivity of piezoelectric scanners scan very slightly throughout the epxeriment. This effect is called hysteresis [9].

Scanning tunneling microscopy offers several advantages over other microscopy techniques [1]. It is able to achieve atomic resolution and image individual atoms and molecules. Furthermore, it is able to modify the surface by manipulating single atoms. In a famous experiment, researchers were able to write the letters IBM using individual xenon atoms deposited on nickel [12]. STM is able to work with a large variety of materials in different mediums. It operates both under ultra-high vacuum (UHV) or ambient conditions, at very low and high temperatures and samples can even be immersed in liquids. Hardly any sample preparation is usually required for STM and the technique is non-destructive. It also allow for real-time surface studies, and STM is thus particularly useful in imaging dynamic processes. Lastly, it allows for researchers to study the unique surface of a compound, as opposed to studying the average properties of bulk materials such as in X-ray crystallography. The main drawback of STM is that it requires the samples to be electrically conductive.

QUANTUM TUNNELING

As mentioned before, tunneling refers to the ability of electrons to 'tunnel' or travel through a barrier that would be classically forbidden. The effect originates from the wave-like nature of electrons. In quantum mechanics, particles can be fully described in quantum mechanics using their wavefunction, which is a solution to the Schrödinger Equation. A full introduction to quantum mechanics relevant to physical chemistry cannot be given here, but can be found elsewhere [5].

Quantum tunneling can best be described by briefly considering the following example of a particle penetrating a rectangular potential energy barrier. If a particle with energy E travelling towards the barrier, the particle will be reflected if E is smaller than the potential energy barrier V. This can be compared with a rollercoaster cart not being able to travel over a hill if the kinetic energy of the cart is smaller than the gravitational energy barrier imposed by the hill. In quantum mechanics, there is some probability for the particle to be found on the other side (see Figure 4). Instead of overcoming the barrier, the particle is said to have tunneled *through* the barrier. Tunneling is described by the probability that an incident wave to the barrier will tunnel through the barrier instead of being reflected (see Figure 5).

The oscillating wavefunction of the incident particle is sinusoidal outside the barrier, but inside the barrier there are no oscillations and the wavefunction decays exponentially. Given that the function is non-zero at the opposite side, an oscillating wavefunction will result again on the other side of the barrier. This effect only occurs when the function is non-zero at the other side of the barrier and thus the barrier should be sufficiently thin for tunneling to occur.

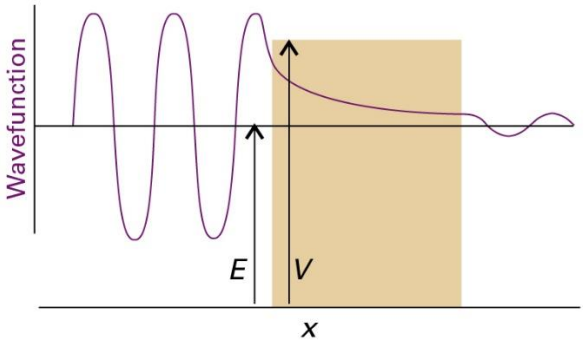

Figure 4. A wavefunction incident on a barrier will decay exponentially within the barrier with the possibility of forming an oscillating wavefunction on the other side of the barrier [5].

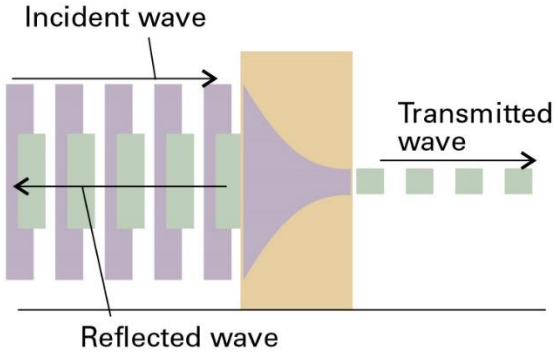

Figure 5. An incident wave on a barrier has a finite probability to tunnel through the barrier (transmitted wave) or to be reflected [5].

In STM, the conducting tip and sample represent the region outside of the barrier. The gap between the tip and the sample is the tunneling barrier. When the electron wavefunctions of the tip and the sample overlap, the barrier will be penetrated and a tunneling current will be created [4]. A physical explanation can be given using density of states (DOS); the amount of electrons at a specific energy level. STM uses a bias to probe this local density of states (LDOS) of the sample. STM thus does not 'feel' the atoms directly, but rather their electron distribution. Depending on the polarity of the bias, electrons tunnel from occupied tip states to unoccupied sample states or vice versa. Both the tunneling probability as the tunneling current are strongly depend on the tip-sample distance. The atom of the tip that is closest to the sample will thus carry the majority of the tunneling current, hence the large distance dependence which explains the high resolution STM can achieve. Normally, when the tip and sample are in thermal equilibrium, the net tunneling current will be zero since the tunneling flow from the tip to sample will be equal to the tunneling flow from the sample to the tip. In STM, a bias is applied to generate a tunneling current. Tunneling theory relevant to STM was developed most notably by Bardeen [13] and explicitly applied to STM by Tersoff & Hamann [14]. Two approaches to calculating the tunneling current will be given here.

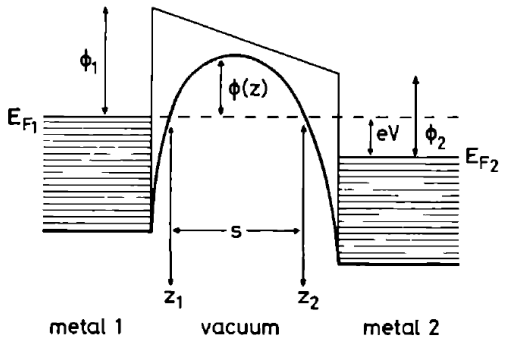

Figure 6. Metal-insulator-metal model with a bias applied to metal 2 with barrier height ϕ (z), Fermi levels E_{F1} and E_{F2}, work functions ϕ_1 and ϕ_2, and barrier width $s = z_2 - z_1$ (here s=d) [8].

Let us consider two metal electrodes separated by an insulator where a bias is applied to one electrode at T = 0 K (see Figure 6). The electron states of both electrodes are filled up to their Fermi level, which can be defined as the level of the highest occupied electron level at T =0 K. This metal-insulator-metal model serves as a model for tunneling in STM if the bias voltage is small and the distance d not too large [1,8]. In this case, there will be a net flow of electrons from left to right because there are electron states available to which they can tunnel. Only electrons with an energy between the two Fermi energy levels will contribute to the current. The probability for tunneling to occur in STM is given by:

$$P \propto e^{-2kd} \quad \text{where} \quad k = \sqrt{2m(V-E)/\hbar^2} \quad (1)$$

and is indeed strongly dependent on the tip-sample distance *d*. The tunneling current is in this case defined by:

$$I = e \int D(E_z)\, n(E_z)\, d(E_z) \qquad (2)$$

Where $D(E_z)$ is the tunneling probability for a barrier of height $\phi\ (z)$ and $n(E_z)$ is the number of incident electrons to the barrier with energy E_z. $D(E_z)$ is given by using the Wentzel–Kramers–Brillouin approximation:

$$D(E_z) = exp\left\{\frac{-4\pi}{h}\int_{z_1}^{z_2}\sqrt{2m[(\phi(z) + E_F) - E_z]}dz\right\} \qquad (3)$$

$n(E_z)$ can be calculated by using the Fermi-Dirac distribution:

$$n(E_z) = \frac{2m^3}{\hbar^3}\iint_{-\infty}^{\infty}\left[f(E_{z)} - f(E_z + eV)\right]dv_x dv_y \qquad (4)$$

In the case of STM, Eq. 3 and 4 these can be incorporated into Eq. 2 and approximated as:

$$I = \frac{e}{4\pi^2\hbar d^2}\left[\phi e^{-A\sqrt{\phi}d} - (\phi + eV)e^{-A\sqrt{\phi+eV}d}\right] \text{ with } A = \frac{2\sqrt{2m}}{\hbar} = 1.025\ eV^{-1/2}\text{Å}^{-1} \qquad (5)$$

This describes the net flow of particles by subtracting the right-left flow from the left-right flow. The equation can still be simplified further by assuming that $eV \ll \phi$, which is the case in STM where the applied voltage is small. The formula than reduces to:

$$I = \frac{e}{8\pi^2\hbar^2}\frac{A\sqrt{\phi}}{d}e^{-A\sqrt{\phi}d} \qquad (6)$$

Or more simply $I \propto (V/d)e^{-A\sqrt{\phi}d}$. In STM, typically the change of 1Å in gap distance results in a change in the tunneling current of around an order of magnitude [15].

An alternative approach to the tunneling current problem in STM would be to use Bardeen's formalism which gives an approximate expression for the tunneling current:

$$I = \frac{2\pi}{\hbar}\sum_{\mu\nu} f(E_\mu)[1 - f(E_\nu + eV)]\left|M_{\mu\nu}\right|^2 \delta(E_\mu - E_\nu) \quad (7)$$

where $f(E)$ is the Fermi function, V the applied voltage, $M_{\mu\nu}$ the tunneling matrix element between states φ_μ of the tip and φ_ν of the sample and E_μ and E_ν respectively the energy of these states in the absence of tunneling [1,14]. The tunneling current is thus given by a combination of the local density of states of the tip and the sample. The essential problem here is to determine $M_{\mu\nu}$, the relative weight of these two elements. Bardeen solves this problem by modelling the tip as locally spherical. For simplicity, let us consider the tip to be a point probe with the tip wave functions localized, the matrix element $\mathrm{M}_{\mu\nu}$ will be proportional the amplitude of φ_ν at a position $\bar{r}_0$. Equation 7 than reduces to:

$$I \propto \frac{2\pi}{\hbar}\sum_\nu |\varphi_\nu(\bar{r}_0)|^2 \delta(E_\nu - E_F) \quad (8)$$

Where the right-hand side of the equation represents the charge density from states at the Fermi level (local density of states, LDOS). The tunneling current is thus proportional to the LDOS of the surface at the positon of the tip. This means that the STM image represents the contour map of the constant surface LDOS, which is indeed the case. Via a more formal mathematical derivation of the matrix element equation, Bardeen found that the tunneling matrix ($\mathrm{M}_{\mu\nu}$) is given by the integrating the current operator over the surface of the barrier region:

$$\mathrm{M}_{\mu\nu} = \frac{\hbar^2}{2m}\int d\bar{S}\left(\varphi_\mu^* \bar{\nabla}\varphi_\nu - \psi_\nu \bar{\nabla}\varphi_\mu^*\right) \quad (9)$$

TIP CHARACTERIZATION AND PERFORMANCE

Two factors characterize tip performance in STM: geometric characteristics and material characteristics. Various metals can be used for STM tips. Tungsten (W), Platinum (Pt) or Platinum-Iridium (PtIr) tips are used commonly in STM. Under ambient conditions, PtIr tips are usually preferred since such tips, a contrary to tungsten tips, are not easily oxidized. Oxidation and other contaminations have a disadvantageous effect on the tip quality and thus image quality. In vacuum, tungsten tips are usually preferred since these are generally cheaper and easier to produce [9]. The geometrical characteristics of influence are the aspect ratio, radius of curvature, opening angle and shape of the tip (see Figure 7) [16,17]. The aspect ratio is defined as length to base width (L/W). Short tips are required for STM imaging in order to decrease mechanical vibrations that blur the image [16]. The radius of curvature should be as small as possible in order to produce images with high resolution. The opening angl e is of influence to the tip broadening effect. The tip should be spherically symmetrical in order to produce well-defined electronic wave functions leading to an undistorted image. Lastly, the tip should also be stable under high electric fields [9]. Ideally, the tip is only one atom wide at the apex (atomically sharp).

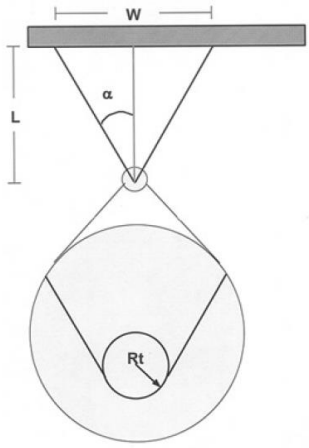

Figure 7. Key parameters in an idealized spherical tip. Here W and L represent the width and length respectively, α the opening angle and R_t the radius of curvature of the tip [17].

The quality and characteristics of the tip have a direct effect on the image quality obtained. 'Tip artefacts' are commonly referred to as all tip-related obstacles that prevent us from retrieving an image that perfectly represents the actual surface of the sample. A whole class of tip artifacts exist, of which some are related to the geometric characteristics of the tip and some are related to imperfections on the surface of the tip. On the one hand, the inherent geometrical characteristics of the tip can lead to images that do not perfectly represent the surface of the material being studied. These are often the result of the relative size of the tip compared to trenches and holes present at the surface. The tip is often not able to fully penetrate holes (trench width reduction effect) nor to accurately image small protrusions (tip broadening effect). Examples of this are visible in Figure 8 and 9.

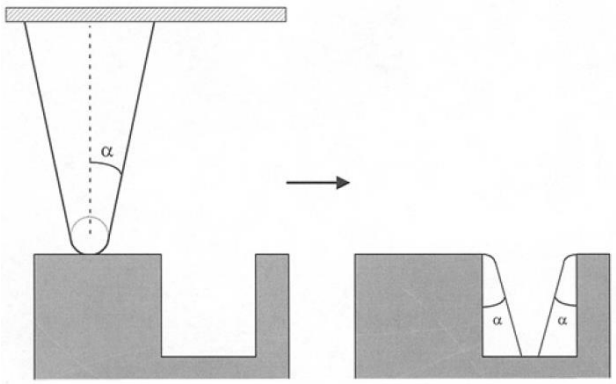

Figure 8. Trench width reduction effect [17].

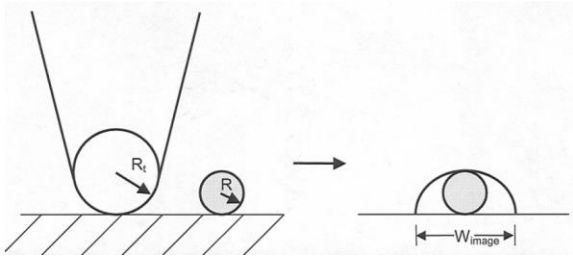

Figure 9. Tip broadening effect [17].

On the other hand, image artefacts due to non-ideal geometric shape of the tip can for example lead to 'ghosting' of images by which the image becomes blurry (see Figure 10). These defects can be due to the production process or develop while being in use. 'Double tips' can for example disturb the tunneling current and lead to ghosted double tip imaging. Correcting for these factors in the post-processing can lead to improved images although it remains difficult to assess how well the image represents the surface [17].

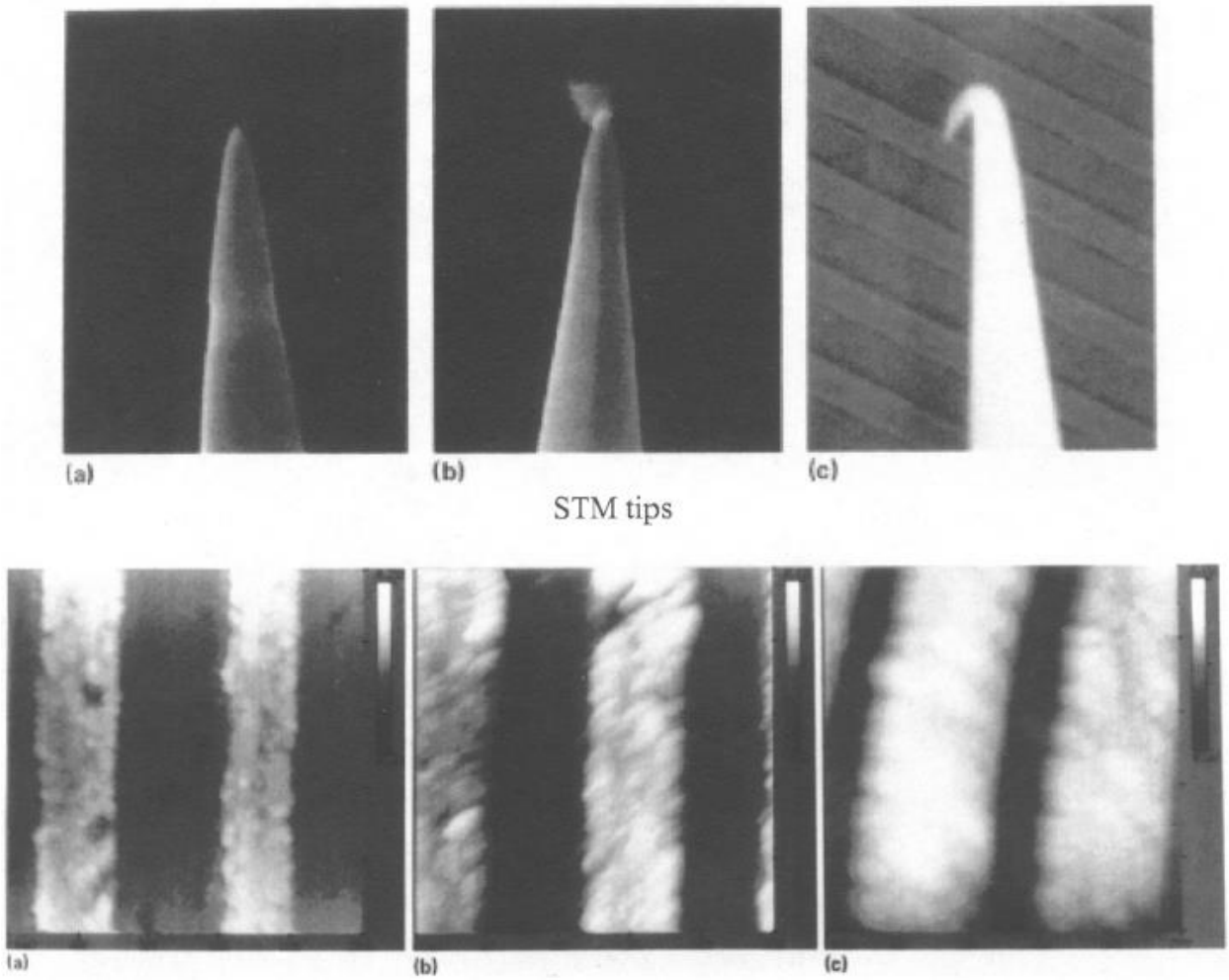

Figure 10. Scanning Electron Microscope (SEM) images of STM tips, with (a) an undamaged and clean tip, (b) a contaminated tip and (c) a damaged tip. Corresponding STM images are shown, in which the effect of damage and contamination of tips is clearly visible. The pictures are illustrative, since tip and image dimensions are not shown [17].

PRODUCTION OF ATOMICALLY SHARP TTIPS

Different methods exist that are used to produce STM tips of high quality. Oliva et al. list electrochemical, mechanical, evaporation, cutting and breaking off techniques as methods that are commonly used to produce such tips [16]. Additionally, methods to further sharpen tips after production also exist, but the effect of these techniques is often only determined empirically [9]. For example, resistive heating, in which the tip is (flash) heated to above 800° C, can be used to remove oxide layers and other contaminations [9,18]. High electric field treatments are also used to remove contaminations. In this procedure, the bias voltage used for tunneling is raised significantly for some time [9]. Alternatively, by indenting the tip into a soft metal, a new microtip can be formed that will serve as the tunneling conductor. Conventional sputter sharpening is also used as a post-etching procedure. Combinations of these techniques are also used, for example by Chaicka et al.

Here, the electrochemical etching of STM tips will first be discussed extensively, followed by treatment of (field-directed) sputter sharpening.

ELECTROCHEMICAL ETCHING

Electrochemical etching refers to the process in which a metal wire will partly dissolve in such a way that the remains of the wire will form a sharp tip. By dipping the metal wire into an electrolyte solution containing an electrode and applying a voltage, the process will dissolve the wire partly near the air-solution interface until a sharp tip will have been formed. The voltage is applied in such a way that the wire (tip) is the anode and the submerged electrode is the cathode in this electrochemical etching process. Electrochemical etching is currently the most practical method for producing STM tips because it is able to produce cheap, reliable STM-tips of desired quality while the process is relatively easy and fast. Typical tip radii produced by conventional electrochemical etching range between 4-50 nm [2,19].

Using a micrometer screw, a very thin tungsten wire is partly submerged into a NaOH or KOH electrolyte solution. There does not seem to be a clear preference for either NaOH or KOH in the literature, and solutions of various molarity are used. For example, Guise et al. used a 2M KOH solution, Muller et al. a 2 M NaOH solution, Oliva et al. both NaOH and KOH of various concentrations and Lucier a 7.5 M KOH solution [16,19–21]. Both electrodes are connected to a control unit, which applies a DC bias voltage. The wire is then electrochemically etched until the 'drop-off' takes place and a sharp tip is formed near the solution-air interface. The current is closely monitored to be switched of when this drop-off has occurred. The time period in between the drop-off and the switching off of the applied voltage is called the cut-off time. Typically, the tungsten wire will have a diameter of around 0.3 mm, the applied voltage is around 3V and the etching process takes around 10 minutes, although Lucier reports times as short as a couple of minutes and Oliva et al. etching times of up to 50 minutes [16,21].

The chemical reaction of the tungsten dissolution can be expressed as:

$$W\ (s) + 2OH^- + 2H_2O\ \rightarrow\ WO_4^{2-} +\ 3H_2\ (g)$$

In other words, the tungsten wire is oxidized to form tungstate anions which are soluble in water, and thus the wire is partly dissolved. The question remains however, why a sharp tip is formed during this process.

The tip is formed during the etching process because the electrolytic solution's surface tension will form a meniscus around the tungsten wire emerged in it. The concentration of OH^- ions is lower near the top of the meniscus than in the solution overall. Thus, the etching process takes place at a slower rate at the top of the meniscus. Where etching takes place at a higher rate, tungsten anions are formed that will flow downwards. This hinders the electrochemical etching of the tungsten wire submerged below the meniscus. Thus, a so-called 'neck-in' will occur close to the bottom of the meniscus. Eventually, the submerged part of the tungsten wire will become too heavy and the drop-off occurs. At the breaking point, the sharp tip is formed. The formation and shape of the meniscus is thus crucial for

electrochemical etching. It was experimentally confirmed that altering the meniscus shape, e.g. by lifting the wire during the process, will also alter the shape of the tip [2]. Because of the crucial shape of the meniscus, the production process should be kept free of external vibrations. The neck-in and drop-off process is depicted in Figures 11 and 12.

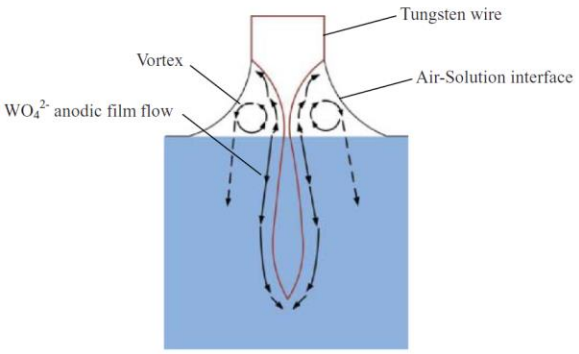

Figure 11. Neck-in process due to the tungsten anion flow around the meniscus [2].

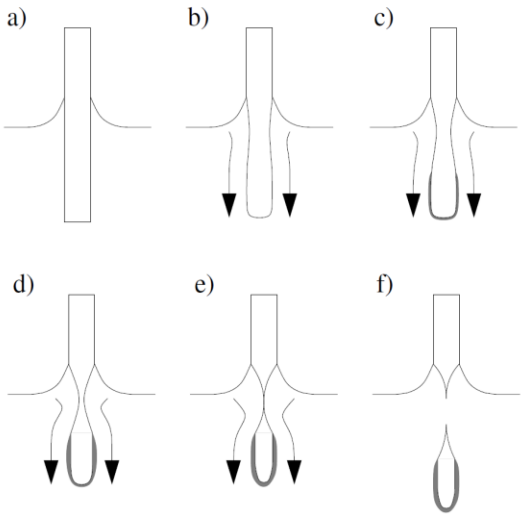

Figure 12. The drop-off process as a result of the neck-in process and the weight of submerged wire. The meniscus is formed in a), b) to e) show the tungsten anion flow and f) the drop-off [21].

After etching, the tip has to be cleaned. Researchers report different methods in order to do so. Rinsing with distilled water seems to be standard and most papers report rinsing with methanol or ethanol afterwards. Gentle drying with clean compressed nitrogen gas is reported by Lucier, Oliva et al. report the use of an ultrasonic cleaner combined with distilled water [16,21]. Chaika et al. reports the report the use of hot distilled water since ultrasonic rinsing in ethanol or acetone potentially leads to breaking the tip apex [18].

One of the many things that makes electrochemical etching particularly challenging, is the fact that the process is not self-limiting and continuing to apply the voltage after the drop-off has occurred, will adversely affect the tip sharpness. Most papers describe a mechanism that automatically cuts of the applied voltage within 500 ms after the drop-off has occurred. This is possible because of a sharp drop in current after the drop-off, as depicted in Figure 13. However, Guise et al. found that turning the power supply off is in itself not sufficient to create sharp tips [20]. The problem is that even without an applied voltage, a small natural work function bias exists in the electrolytic solution and thus continues to etch the tip. This process will adversely affect the sharpness of the tip and blunt it (see Figure 14). They found that by applying a reverse bias, the electrochemical reaction could be frozen, prohibiting the natural bias from further blunting the produced tip.

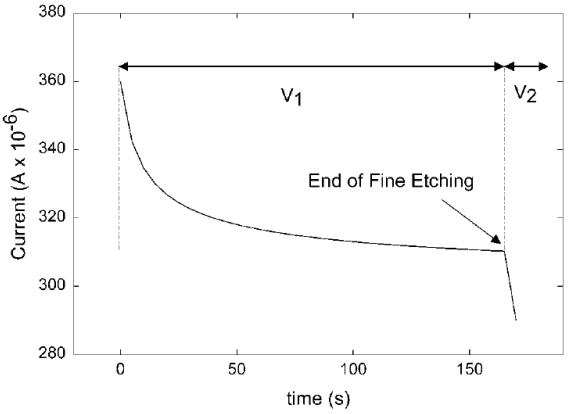

Figure 13. Evolution of the current during electrochemical etching. The end of fine etching depicts the drop-off moment and activates the power supply switch-off [20].

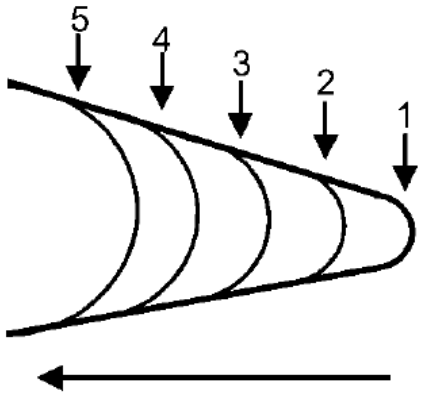

Figure 14. Schematic depiction of post-etching blunting of the STM tip as time evolves [20].

Another method to prevent blunting is to connect a reservoir of deionized water to the solution and flush the electrolytic solution with deionized water immediately when the drop-off has occurred. Additionally, the lower part of the tungsten wire also forms a tip at the drop-off, and the blunting process does not affect this submerged STM-tip [19]. By designing the production device in such a way that these submerged tips are recollected undamaged, sharp tips can also be produced.

Most papers describing electrochemical etching procedures are using a tungsten wire. The low chemical reactivity of PtIr which makes them less inert to oxidation than tungsten does require the use of dangerous chemicals to successfully etch the tips [21]. Besides the oxidation problem preventing tungsten tips from being used under ambient condition, the storage of these tips after production is also problematic: oxidation will take place if stored under ambient conditions [19]. This does not only affect the sharpness of the tip, but could destabilize the tunneling current as well [16]. Both Muller & Guise report an oxidation layer on the tip of around 2nm thickness.

Most research papers covering electrochemical etching of tungsten tips have sought under which characteristic parameters the best (sharpest) tips are produced. Oliva et al. report best results with KOH as electrolyte and an applied voltage between 2-6 V [16]. Furthermore, the sharpest tips resulted from those where a large part of the wire was submerged. This effect is due to the larger weight of the part that is dropped off. They did not find a relation between the diameter of the wire used and the tip sharpness, only between wire diameter and tip length. Because optimal tips must be short, the wire used should not have a too small diameter.

Lucier reports that a short meniscus will result in a small aspect ratio of the tip [21]. When it comes to the effect of the length of the wire submerged, the report finds it to be ambiguous and states that this effect is still uncertain. An applied voltage of around 3V (DC) was found to be optimal in this particular research. Furthermore, the concentration of the electrolyte solution is also of influence and since both a too high as too low concentration are disadvantageous, a balance has to be found. This will most likely differ from set-up to set-up [21].

SPUTTER SHARPENING

An alternative tip production method was introduced by Schmucker et al. in 2012, the so-called *field-directed sputter sharpening* (FDSS) [22]. The principle behind this production technique is quite simple; a tip is sharpened by shooting ions at the tip with considerable kinetic energy and sputter erosion takes place at the surface of the tip (*sputter sharpening*). By applying a voltage to the tip, the ions are deflected in such a way by the tip that a very sharp tip will be formed (*field directed*). This new technique is promising to researchers because of multiple reasons. Firstly, the process is self-limiting and does not require oversight. Secondly, the technique is suitable for batch production. Thirdly, it is efficient and cheap. Lastly, it produces tips of high(er) quality than previous methods.

Conventional sputter erosion (CSE) can also be used to sharpen metallic tips, but cannot produce the sharp tips needed for STM [22]. In CSE, the sharpening takes place due to the angle of incident of the ions bombarded at the tip. It can be used to remove contaminations from the surface of the tip [16]. It is comparable to ion milling, in which an ion beam is aimed at the tip under production while rotating said tip [23]. Chaicka et al. used sputter sharpening in combination with other techniques to produce well-defined nanoscale pyramidal tungsten tips. Tips were produced using electrochemical etching in 2M NaOH, without applying reverse bias. Afterwards, the tips were further sharpened by electron beam heating (flash heating) and ion sputtering. The ion sputtering was performed using a 600 eV argon ion beam applied for 15-20 minutes. The sharpening procedure was carried out in the UHV chamber of a scanning tunneling microscope under room temperature without applying any bias to the tip.

Schmucker et al. were able to produce tungsten tips with sharper tips than conventional methods by using Field-Directed Sputter Sharpening, as can be inferred from Table 1. The field-directed sputter sharpening takes places in a high-vacuum chamber. Schmucker et al. report a background pressure below $5 \cdot 10^{-8}$ Torr. The temperature of the tip was not controlled, and the tip was placed at 5-10 cm from the focusing assembly of the ion gun (nominal beam diameter: 2mm). Further details on the exact ions used, ion energy and bias applied can be found in Table 1.

Table 1: Experimental field-directed sputter sharpening parameters and results of Schmucker et al. [22].

Tip material	Ion compound	Ion energy	Bias	Final radius	Duration
PtIr (90/10%)	Neon	2.0 KeV	400V	<1 nm	195 min
Tungsten	Argon	1.5 KeV	150 V	2-3 nm	1 hr
Tungsten + hafnium diboride coating	Argon	1.2 KeV	200 V	4 nm	60 min

In FDSS, a positive bias is applied to the tip. This produces a spatially localized repulsive potential at the apex of the tip (see Figure 15). The electric field gets stronger as the apex narrows, thus ions directed at the sharpest part of the tip will undergo the most deflection [24]. This subsequently leads to an even further reduction of the ion flux at the apex which produces a sharp apex due to directed sputter sharpening. The effective ion impact energy is the difference between the tip bias and the accelerating voltage of the ion gun. Schmucker et al. have performed computer simulations of the ion sputtering [22]. Their model shows a dependence of the relative ion flux (flux reduction in the apex region) on the ratio between tip bias to ion accelerating voltage (V_r). This dependence follows a square root relation (see Figure 16).

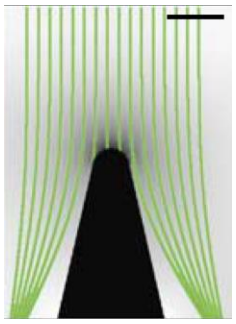

Figure 15. Simulation of field-directed sputter etching around a biased tip apex for V_r = 0.44. (greyscale represents strength of electric field, green lines the paths of individual ions, scale bar: 20 nm) [22]

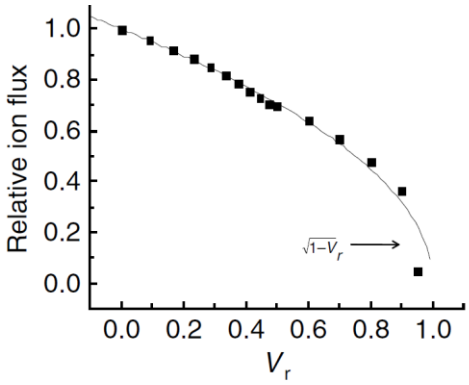

Figure 16. Relative ion flux in the apex region vs. V_r (ratio tip bias/ion accelerating voltage). The dependence shows a root square relation [22].

In comparison to CSE, FDSS produces significantly sharper tips [25]. In CSE, there is a competition between erosional sharpening and blunting of the tip. By field-direction, FDSS produces an equilibrium curvature of the tip that depends on the ion flux and thus on V_r. The deflection of ions also preserves the structural integrity of the tip base which is of importance to tip stability. Ultimately, a tip apex equilibrium is reached in FDSS where ion sputtering continues without influencing the apex. This is the reason that the process is self-limiting and thus does not require manual oversight. Because the process of producing STM tips by FDSS it so simple and effective, it is of great interest to researchers working with STM. Schmucker & Lyding have filed a patent on the technique and founded a company aimed at the production of STM tips using FDSS [26,27].

RESEARCH TOPIC

This research will focus on reproducing the method of STM tip production by field-directed sputter sharpening. Although Schmucker et al. were able to show that field-directed sputter sharpening is able to produce sharp tips consisting of different materials under varying conditions, they have not researched systematically under which conditions the best tips are formed. This research will apply the field-directed sputter sharpening method to readily available tungsten tips. Tips will be produced using Argon ions while systematically varying the tip bias and ion kinetic energy from sample to sample. By doing so, the optimal circumstances can be sought for tungsten tip production using FDSS.

The tip quality will be assessed mainly on the basis of their geometric characteristics using electron microscopy. STM images based on a tip treated with FDSS will also be compared to STM images based on a tip that has not been treated with FDSS. This can be done using a standard STM sample, such as a silicon (111) 7x7 surface. If time allows, the same set of experiments while varying tip bias and ion kinetic energy can be done using a different tip material or ion source.

REFERENCES

[1] Bai, C., Scanning Tunneling Microscopy and Its Applications. Berlin: Springer-Verlag (1992).

[2] Ju, B.F., Chen, Y.L., Ge, Y., The art of electrochemical etching for preparing tungsten probes with controllable tip profile and characteristic parameters, *Rev. Sci. Instrum*. 82 (2011). doi:10.1063/1.3529880.

[3] Wiesendanger, R., Güntherodt, H.-J., *Introduction* in: Scanning Tunneling Microscopy I: General Principles and Applications to Clean and Adsorbate-covered Surfaces (Volume 1) (Edited by: Güntherodt, H.-J., Wiesendanger, R.). Berlin: Springer-Verlag, 1992.

[4] Chen, C.J., Introduction to Scanning Tunneling Microscopy (Second Edition). Oxford: Oxford University Press (2008).

[5] Atkins, P., de Paula, J., Friedman, R., Quanta, matter, and change: a molecular approach to physical chemistry (Second Edition). Oxford: Oxford University Press (2014).

[6] Binnig, G., Rohrer, H., Gerber, Ch., Weibel, E., Tunneling through a controllable vacuum gap, Appl. Phys. Lett. 40 (1982) 178–180. doi:10.1063/1.92999.

[7] Binnig G., Roher, H., Scanning tunneling microscopy —from birth to adolescence, Rev. Mod. Phys. 59 (1987) 615–625. doi:10.1103/RevModPhys.59.615.

[8] Walle, G. van de, Scanning tunneling microscopy: principle, construction and applications (PhD Thesis, Katholieke Universiteit Nijmegen: Nijmegen). Meppel: Krips Repro (1986).

[9] Voigtländer, B., Scanning Probe Microscopy: Atomic Force Microscopy and Scanning Tunneling Microscopy. Berlin: Springer-Verlag (2015).

[10] Tersoff, J., Lang, N.D., *Theory of Scanning Tunneling Microscopy* in: Scanning Tunneling Microscopy (Edited by Stroscio, J.A., Kaiser, W.J.). London: Academic Press Limited (1993).

[11] Binnig G., Rohrer, H., Gerber, Ch., Weibel, E., Surface studies by Scanning Tunneling Microscopy, Phys. Rev. Lett. 49 (1982) 57–61. doi:10.1103/PhysRevLett.49.57.

[12] Eigler, D.M., Schweizer, E.K., Positioning Single Atoms With A Scanning Tunneling Microscope, Nature. 344 (1990) 524–526. doi:10.1038/344524a0

[13] Bardeen J., Tunnelling from a many-particle point of view, Phys. Rev. Lett. 6 (1961) 57–59. doi:10.1103/PhysRevLett.6.57.

[14] Tersoff, J., Hamann D.R., Theory of the scanning tunneling microscope, Phys. Rev. B. 31 (1985) 805–813. doi:10.1103/PhysRevB.31.805.

[15] Kuk, Y., *STM on Metals* in: Scanning Tunneling Microscopy I: General Principles and Applications to Clean and Adsorbate-covered Surfaces (Volume 1) (Edited by: Güntherodt, H.-J., Wiesendanger, R.). Berlin: Springer-Verlag, 1992.

[16] Oliva, A.I., Romero G., A., Peña, J.L., Anguiano, E., Aguilar, M., Electrochemical preparation of tungsten tips for a scanning tunneling microscope, Rev. Sci. Instrum. 67 (1996) 1917-1920. doi:10.1063/1.1146996.

[17] ASTM International, Guide to Scanner and Tip Related Artifacts in Scanning Tunneling Microscopy and Atomic Force Microscopy, (2012) 1–18.

[18] Chaika, A.N., Orlova, N.N., Semenov, V.N., Postnova, E.Yu., Krasnikov, S.A., Lazarev, M.G., ... & Shvets, I.V., Fabrication of [001]-oriented tungsten tips for high resolution scanning tunneling microscopy., Sci. Rep. 4 (2014) 3742. doi:10.1038/srep03742.

[19] Müller, A.-D., Müller, F., Hietschold, M. Demming, F., Jersch, J. Dickmann, K., Characterization of electrochemically etched tungsten tips for scanning tunneling microscopy, Rev. Sci. Instrum. 70 (1999) 3970–3972. doi:10.1063/1.1150022.

[20] Guise, O.L., Ahner, J.W., Jung, M.C., Goughnour, P.C., Yates, J.T. Reproducible Electrochemical Etching of Tungsten Probe Tips, Nano Lett. 2 (2002) 191–193. doi:10.1021/nl010094q.

[21] Lucier, A. Preparation and Characterization of Tungsten Tips Suitable for Molecular Electronics Studies (MSc Thesis, McGill University: Montréal), (2004).

[22] Schmucker, S. W., Kumar, N., Abelson, J. R., Daly, S. R., Girolami, G. S., Bischof, M. R., ... & Lyding, J. W. (2012). Field-directed sputter sharpening for tailored probe materials and atomic-scale lithography, Nat. Commun. 3 (2012) 935. doi:10.1038/ncomms1907.

[23] Park, S., Barret, R.C., *Design considerations for an STM System* in: Scanning Tunneling Microscopy (Edited by Stroscio, J.A., Kaiser, W.J.). London: Academic Press Limited (1993).

[24] News Bureau, University of Illionois (Ahlberg, L.), Microscope probe-sharpening technique improves resolution, durability (07 May 2012). (Accessed May 01, 2015 from: http://www.news.illinois.edu/news/12/0705probes_JosephLyding_GregGirolami.html).

[25] Schmucker, S.W., Sharpening of Conductive Nanoprobes for Scanning Tunneling Microscopy by Field-Directed Sputter Sharpening (MSc Thesis, University of Illinois: Urbana-Champaign), (2009).

[26] Tiptek, Tiptek - Home Page, (n.d.). (Accessed May 08 2015 from : http://www.tiptek.com/Home_Page.html).

[27] Lyding, J. W., & Schmucker, S. W. (2011). *U.S. Patent No. 8,070,920*. Washington, DC: U.S. Patent and Trademark Office